Shear wave velocities across the olivine – wadsleyite – ringwoodite transitions and sharpness of the 410 km seismic discontinuity

Jean-Philippe Perrillat, Benoît Tauzin, Julien Chantel, Julie Jonfal, Isabelle Daniel, Zhicheng Jing, Yanbin Wang

Version of Record: https://www.sciencedirect.com/science/article/pii/S0012821X22003260
Manuscript_b59b9bfc1464a8696d848fe81cecbcce

Shear wave velocities across the olivine – wadsleyite – ringwoodite transitions and sharpness of the 410 km seismic discontinuity

Jean-Philippe Perrillat,*[1] Benoît Tauzin,[1,2] Julien Chantel,[3] Julie Jonfal,[1] Isabelle Daniel,[1] Zhicheng Jing,[4†] and Yanbin Wang,[4].

[1] Université de Lyon, Université Lyon 1, Ens de Lyon, CNRS, UMR 5276 Lab. de Géologie de Lyon, Villeurbanne F-69622, France
[2] Research School of Earth Sciences, Australian National University, Canberra, Australian Capital Territory 0200, Australia
[3] Univ. Lille, CNRS, INRAE, Centrale Lille, UMR 8207 - UMET - Unité Matériaux et Transformations, F-59000 Lille, France
[4] Center for Advanced Radiation Sources, The University of Chicago, Chicago, Illinois 60637, USA
[†]Now at: Department of Earth and Space Sciences, Southern University of Science and Technology, Shenzhen, Guangdong, China

Corresponding author:
Dr Jean-Philippe Perrillat – jean-philippe.perrillat@univ-lyon1.fr
Postal address: Laboratoire de Géologie de Lyon UMR5276, Université Lyon 1, 2 Rue Raphaël Dubois, Villeurbanne F-69622, France

Keywords: olivine, wadsleyite, ringwoodite, kinetics, seismic discontinuity, Earth's mantle

Highlights:

- We report X-ray diffraction and sound velocities across the olivine transition
- Shear waves exhibit a transient velocity softening and attenuation
- This transformational softening may arise from a metastable spineloid phase
- This could explain the sharpness and reflectivity of the 410 km discontinuity

Abstract

The seismic signature of the 410-km seismic discontinuity is generally attributed to the olivine to wadsleyite polymorphic transformation. However, apparent discrepancies exist between seismic and experimental observations. Among those, the sharpness of the discontinuity as inferred from the reflectivity of seismic waves is difficult to reconcile with the gradual nature of the olivine to wadsleyite transformation predicted by phase equilibria. In this study, we explore the contribution of the phase transition kinetics to the sharpness of the discontinuity by performing X-ray diffraction and sound velocity measurements on $(Mg,Fe)_2SiO_4$ with an unprecedented time resolution as a function of the reaction progress. Our data document for the first time a transient velocity softening phenomenon and attenuation which we relate to the formation of a metastable spineloid phase. In the Earth's mantle this transformation mechanism would affect the elastic gradient within the olivine-

wadsleyite two-phase loop, potentially creating a low-velocity layer; hence explaining the unique sharpness and reflectivity of the discontinuity.

1. Introduction

Olivine, $(Mg,Fe)_2SiO_4$, is the most abundant mineral in the upper mantle. Its transformations to wadsleyite and ringwoodite are responsible for the seismic discontinuities observed at 410 and 520 km depths, respectively. Knowing the transformation pressure and kinetics, as well as the variation in density and elasticity associated with these transitions is essential to understanding the depth, sharpness, and amplitude of these discontinuities. These seismic properties also impose critical constraints on the composition and structure of the Earth's mantle, with profound geodynamic implications. In global seismic Earth models, the 410-km discontinuity (hereafter referred to as d410) is characterized by an abrupt rise velocity of about ~ 5% in PREM (Dziewonski and Anderson, 1981) and ~ 4% in AK135 (Kenneth et al., 1995). In regional studies, the large amplitude of short-period (~1 Hz) reflected seismic waves reveals that most of the energy of the seismic waves is reflected from a narrow zone, in some cases 4 km or less in thickness (Benz and Vidale, 1993; Yamazaki and Hirahara, 1994, Neele, 1996; Tibi and Wiens, 2005; Waszek et al., 2021). Although these seismic estimates may suffer from intrinsic uncertainty related to focusing effects, such a sharpness is inconsistent with a phase transition in a solid solution Mg_2SiO_4-Fe_2SiO_4 that occurs over a large range of pressures depending on the composition. Thermodynamic and mineralogical models estimate the width of the transformation loop to be 7-19 km thick for typical mantle temperature and composition (Akaogi et al., 1989; Katsura et al., 2004, 2010). As a consequence, several additional constraints have been proposed to resolve this discrepancy with the seismic observations. The strong curvature in the binary loop boundaries could result in a non-linear gradient in mineral transformation yields, and hence in elastic properties across the tranformation (Gaherty et al., 1999). This could lead to a sharper d410 in seismic observations (Helfrich and Wood, 1996; Stixrude, 1997). Fe-Mg partitioning involving non-transforming phases, such as garnet, might have a similar effect (Irifune and Isshiki, 1998). Conversely, lower temperature may widen the divariant loop (Helffrich and Bina, 1994); and in places with a high vertical component of mantle flow the latent heat of the transition will result in a broader transformation interval compared to the isothermal case (Frost, 2003). Also, the preferential incorporation of water in wadsleyite stabilizes this phase over a wider range of pressures and temperatures, thereby enlarging the transition pressure interval (Wood, 1995; Helffrich and Wood, 1996; Frost, 2003; Frost and Dolejs, 2007). From OH^- partitioning

between olivine and wadsleyite, Wood (1995) estimated that approximately 0.05 wt% H_2O in the mantle transition zone would imply a 20 km wide discontinuity. For higher water content estimates of 0.9 - 1.4 wt % H_2O (Kelbert et al. 2009; Pearson et al., 2014; Wang et al. 2019) the transition may broaden up to over 30 km for geotherm conditions < 1200°C. With these results, the observation of a 2-10 km-thick d410 in the cold, likely hydrated, Tonga slab area (Tibi and Wiens, 2005) is particularly puzzling, and underlines the need for additional mechanisms for reconciling the widths of phase transitions with those of observed seismic discontinuities.

A yet largely unexplored aspect is the dynamics of mineral transformations. Anomalous elastic behaviors, such as softening (*i.e.* reduction of elastic moduli), have been reported in the vicinity of phase transitions of some minerals (e.g., Carpenter and Salje, 1998;, Lakshtanov et al*.,* 2007) and may cause variations in both P- and S-wave velocities. The presence of a metastable phase might also affect the acoustic signature of a transition, as observed in orthopyroxene (Kung et al., 2004; Zhang et al. 2013; Zhang and Bass 2016; Wang et al. 2019). In the olivine system, the existence of intermediate phases between high-pressure polymorphs has been predicted by transformation models, and would derive from a shear-induced reaction mechanism where the *hcp* oxygen sub-lattice in olivine is sheared, via stacking faults, into the *fcc* configuration in wadsleyite and ringwoodite (Hyde et al., 1982; Madon and Poirier, 1983, Bassett and Skalwold, 2021). The process would either lead to the so-called spineloid ε-phase (Madon and Poirier, 1983), or to a disordered spineloid in the case the arrangement of the cation sublattice is not achieved (Guyot et al., 1991). The ε-phase has been recently identified by X-ray diffraction (XRD) in quench products from the olivine to ringwoodite transformation (Chandler et al., 2021); while the disordered spineloid has been identified *in situ* during time-resolved measurements across the olivine – wadsleyite and olivine –ringwoodite transitions. In this latter case, XRD patterns are characterized by the preferential growth of the diffraction lines corresponding to the *fcc* oxygen sublattice, because of the lack of long-range order for the cations. This feature was first observed by Furnish and Bassett (1983) and Chen et al. (2001) in Fe_2SiO_4, as well as Will and Lauterjung (1987) in the Mg_2GeO_4 system. It was subsequently reported in the $(Mg_{0.9}Fe_{0.1})Si_2O_4$ mantle composition by our group (Perrillat *et al*., 2013, Perrillat *et al*., 2016; where it is referred as γ*phase) and confirmed by Rosa *et al*. (2016). The presence of an intermediate metastable spineloid phase therefore appears to be a robust feature of the olivine high-pressure transitions, as confirmed by the recent discovery of ε-Mg_2SiO_4 in the heavily shocked Tenham meteorite (Tomioka and

Okuchi, 2017; Tomioka et al., 2021) named “poirierite” in honour of Jean-Paul Poirier. Investigation of the seismic effect of this transient phase is therefore essential for a better understanding of the complex structure of the d410 discontinuity.

In this study, we combine synchrotron time-resolved X-ray diffraction (XRD) and ultrasonic measurements to determine wave velocities as a function of reaction progress across the olivine – wadsleyite – ringwoodite transitions in $(Mg,Fe)_2SiO_4$ samples. These *in situ* data reveal a significant softening at the onset of transformation that might be attributable to the presence of the intermediate spineloid phase reported in previous studies. We also explore through seismic models the implications of this softening, and conclude that this transient phase affects the velocity gradient within the two-phase loop, potentially creating a low-velocity layer and sharpening the d410 discontinuity. The modeled reflection coefficients show that a ~2 km thick layer with a velocity decrease of -1.5% would generate a distinctive ~1 Hz reflection signal of the $P'_{410}P'$ seismic phases consistent with worldwide observations, that could potentially be detected in short periods receiver functions seismic data.

2. Experimental methods

2.1 Starting material

The starting material consisted of fine-grain polycrystalline specimens prepared by hot-pressing powders ground from either natural San Carlos olivine crystals (run# T1634; X_{Fe}=0.1), or synthetic iron-rich olivine (runs# T1204 & T1633; X_{Fe}=0.52), where X_{Fe}= Fe/(Mg+Fe) denotes the iron molar fraction. These specimens were identical to those previously studied in Perrillat et al. (2003; 2016). While the San Carlos olivine is representative of the Earth’s mantle chemistry, the iron-rich X_{Fe}=0.52 composition was chosen for its lower transformation pressure and wider binary loop of 3 - 4 GPa at 650 – 1350 °C (Akaogi et al., 1989). This iron-rich olivine has been synthesized from a stoichiometric mixture of $MgO–SiO_2–Fe_2O_3$ synthetic oxides and heated at 1250°C for 20 hours in a controlled atmosphere furnace ($CO-CO_2$ gas mixture, $fO_2=10^{-10}$ atm). The purity and chemical homogeneity of both samples were confirmed by Energy Dispersive Spectroscopy (EDS) measurements. Powders were subsequently sintered at 4 GPa and 1000°C for 24 hours in a Paris-Edinburgh press at Université de Lyon in order to achieve a fine 1-10 μm grain size, a very low porosity, and the lack of cracks required for the ultrasonic measurements (**Fig. S1**). Finally, cylindrical samples of 1.0 - 0.8 mm in length and 1.2 mm in diameter were prepared with flat faces polished to mirror quality to be perfectly parallel with an accuracy of ± 1 μm.

2.2 High pressure and temperature experiments

High-pressure and high-temperature experiments were conducted at the 13-ID-D Beamline of GSECARS at the Advanced Photon Source, Argonne, IL using a 1000-ton press and a T-25 multi-anvil module (Wang et al., 2009). Samples were loaded in either 14/8 (run# T1634) or 10/5 ultrasonic (runs# T1204 & T1633) cell assemblies (Leinenweber et al., 2012), composed of an MgO octahedral pressure medium with a tubular graphite or "windowed" rhenium heater, respectively (schematic drawings of the cells can be found in Supplementary **Fig. S2**). Gold foils of 2 μm thick were placed on the top and bottom sides of the olivine cylinder to measure the sample length by radiography (**Fig. S3**). A mixture of NaCl + hBN placed at the back of the sample provided quasi-hydrostatic conditions and served as pressure calibrant (Matsui et al., 2012; Le Godec et al., 2000). The uncertainty in the pressure calculation, from the errors in unit cell measurements and equation of state parameters, was typically ± 0.2 GPa. The temperature was monitored using a W_5Re-$W_{25}Re$ thermocouple in contact with the sample, without correction of the pressure-effect on the electromotive force, leading to a precision of ± 10 °C. For run# T1634, the thermocouple reading was lost during the heating stage so that temperature was estimated from power vs. temperature calibration of the rhenium furnace and may suffer from higher uncertainties up to ± 50°C.

Three experiments were performed at the pressure-temperature conditions for the olivine to transform into its high-pressure polymorphs (**Fig. 1**). Phase equilibrium data show that olivine (α) with X_{Fe}=0.1 transforms into wadsleyite (β) at 12.5 GPa – 800°C, over a pressure interval of ~ 0.2 GPa (Frost, 2003; Katsura et al., 2004, 2010), whereas the iron-rich olivine (α) with X_{Fe}= 0.52 transforms directly to ringwoodite (γ) at a lower pressure, *i.e.* starting at 6.5 GPa, over a wide binary loop of ~ 2.5 GPa (Akaogi et al., 1989; Katsura and Ito, 1989). In each experiment, the olivine samples were first cold-compressed to reach the incipient pressure of either the α-β or α-γ coexistence loop. Temperature was then raised slowly (10°C/min) to 400 – 500 °C and annealed for about 30 to 60 min in order to relax the stress in both the sample and the cell assembly. Finally, a heating ramp was conducted at 400°C/min to reach the target temperatures for kinetic measurements, at 825°C for run# T1204, 800 °C for run# T1633, and 890 °C for run# T1634, respectively.

2.3 *In situ* X-ray diffraction and ultrasonic measurements

X-ray diffraction was used to monitor in real-time the transformation to wadsleyite and ringwoodite under isothermal conditions. *In situ* diffraction was performed in an energy-dispersive mode using the 20 – 120 keV white beam of the 13-ID-D Beamline and a solid-state Ge detector (Canberra®), with a two-theta angle fixed at 6°. The vertical and horizontal widths of the incident beam were 100 x 100 μm, respectively. The collection time was set to 60 s in order to improve the temporal resolution of kinetic measurements. This fast collection was achieved at the expense of the signal to noise ratio of XRD patterns (SNR = 40-80, as defined by the ratio of peak amplitude to root-mean-square noise), but was sufficient to identify the major diffraction lines of the product phases. Although the preferential growth of the diffraction lines of the *fcc* oxygen sublattice, the characteristic feature of the spineloid phase, was not observable, we nevertheless consider that the reaction mechanism involving the metastable spineloid was operational as in previous experiments carried out on the same sample chemistry and P-T conditions (Perrillat et al., 2013, 2016). The degree of transformation as a function of time was further obtained from the relative intensities of the main diffraction lines of olivine (namely (130) (131) (112) (041) (240) lines) and wadsleyite (namely (112) (211) (240) (244) lines) or ringwoodite (namely (220) (311) (400) (440) lines) fitted by Gaussian functions after background subtraction. The uncertainty on the degree of transformation is estimated at ±0.05 from the scattering of the phase proportions obtained from the different diffraction lines. Transformation-time data were analyzed using the general Avrami relation $X(t) = 1 - \exp(-kt^n)$ where t is time and k, n kinetic parameters optimized in a least-square fit. This real-time monitoring proceeded until the relative proportions of minerals in the α+β or α+γ phase assemblages no longer evolved with time.

Ultrasonic measurements were conducted in parallel with the X-ray diffraction to estimate the wave velocities variations across the transformation. For this purpose, a dual mode $LiNbO_3$ piezoelectric transducer was attached to the back of the bottom WC anvil, and used to generate and receive both compressional and shear ultrasonic pulses at 50 and 30 MHz resonant frequencies, respectively. The ultrasonic data acquisition time to get an adequate signal to noise ratio was typically 20 s. The two-way travel times of elastic waves through the sample were determined by the pulse-echo overlap method (**Fig. S4**), and converted into velocities using the sample lengths measured using X-ray radiography based on positions of Au markers, with a resolution of ± 2 μm (**Fig. S3**). This sample length was actually interpolated from the initial and final thicknesses measured by X-ray radiography (**Table S1**) assuming that the sample shortening solely results from the extent of the reaction,

and therefore follows the Avrami's relation estimated from the XRD data. This assumption seems reasonable given the limited plasticity of olivine at these low temperatures < 900 °C and short time scales (Hirth and Kohlstedt, 2003). For compressional waves, the ultrasonic echoes reflected at both ends of the sample were overlapping. As a consequence, V_p could not be determined with confidence, and only the shear waves velocities V_s are further discussed in this work. Considering the uncertainties arising from the sample length ± 2.5 μm and travel time measurements ± 0.5 ns, we estimate the overall uncertainty in the present V_s determination to about 1 % of the nominal values.

This experimental method combining time-resolved X-ray diffraction and ultrasonics provides insights into the relationship between the seismic velocities and the transient crystalline processes across the mineral transformations characteristic of the d410 seismic discontinuity.

3. Results and discussion

3.1 Effect of phase transition on shear velocities

Fig. 2 shows time-series of XRD patterns measured across the α-γ transformation in run #T1204. In all runs, the appearance and growth of the high-pressure phase is accompanied by the decrease in intensity of olivine diffraction peaks. In detail, the volume fraction of olivine shows a steep decrease in the first 10 minutes of the reaction until it achieves a steady state after 30 to 40 minutes. The observed kinetics behavior can be described using the Avrami's relation. At the end of each experiment, the coexistence of olivine with either ringwoodite or wadsleyite evidences the achievement of equilibrium within the two-phase loop. The relatively low degrees of transformation, *i.e.* the persistence of a large fraction of olivine, is explained by the drop in confining pressure of 1.1 to 1.5 GPa due to the negative volume change intrinsic to the reaction: the β and γ phases are 7% and 8% denser than olivine, respectively. The steep decrease in olivine fraction at the onset of transformation is consistent with an early saturation of nucleation sites followed by interface-controlled growth of the product phases, as evidenced in our previous kinetic studies (Perrillat et al., 2013; 2016). The overall transformation timescales are in agreement with the ~ 10^{-9} $m.s^{-1}$ growth rate reported at 870 °C in these earlier works using similar fine-grain polycrystalline olivine samples.

The evolution of ultrasonic velocities with time and reaction progress is shown in **Fig 3**. Shear velocities drop by 80 to 350 $m.s^{-1}$ in the first 3 to 5 minutes of the reaction,

corresponding to a 1.8 to 7.5 % reduction in V_s, respectively, followed by a steady increase that correlates with the duration of the reaction. At the end of the experiments, V_s values agree within uncertainties with velocities calculated from literature elasticity data (see Supplementary **Table S2**) for a mixture of α+β or α+γ phases in the proportions observed in the present XRD measurements (**Fig 3**). The large velocity drop at the onset of the reaction is coupled with a simultaneous lowering of waveform amplitudes, while, afterward S-wave echoes increase again in amplitude after this initial period (**Fig 4**). This initial drop in waveform amplitude reaches 45% for run # T1204, 39 % for #T1633, and 32% for #T1634.

3.2 Softening and attenuation at the onset of transformation

Previous studies have generally focused on the magnitude of velocity jumps across the polymorphic phase transitions of olivine from the equilibrium phase proportions along the transition interval and the elastic moduli of the individual phases (e.g., Gaherty et al., 1996; Weidner and Wang, 2000). Whatever the averaging scheme for the effective elastic moduli calculation and the linear or non-linear rate in the volume fractions of phases one assumes, modeled velocities across the binary loop always take intermediate values between the velocity of olivine and that of its high-pressure form, increasing gradually between these end-member velocities. In contrast, the present measurements show a significant decrease in shear wave velocities in the first steps of reaction. This transient slowness in V_s cannot be explained by thermal effects since the amplitude of velocity drop is much larger than the expected ~150 $m.s^{-1}$ drop caused by a ~ 400 °C temperature jump, based on the temperature derivative dVs/dT of shear velocities of the $(Mg,Fe)_2SiO_4$ polymorphs (Sinogeikin et al., 2003; Liu et al., 2005). Moreover, in our experiments, velocities keep decreasing for a few minutes after temperature is stabilized, arguing for a transformational origin for the velocity drop. An explanation for this velocity reduction might be the formation of the metastable spineloid phase observed in previous works, that would further transform with time into thermodynamically stable wadsleyite or ringwoodite. The velocity softening may result from the highly defected nature of the spineloid, while the lowering of the waveforms amplitudes may track intrinsic attenuation from cations diffusion or scattering of the wave associated to changes in microstructures across the reaction.

3.3 Implications for the sharpness of the 410km discontinuity

The application of the above experimental results to the Earth's mantle requires that we assess the role and extent of the transient spineloid phase in natural geodynamic environments. Due to the gradual transformation of olivine into wadsleyite through the binary loop, a substantial amount of the spineloid phase will be produced continuously over the depths covering the transition. In low temperature subduction settings, due to the slow kinetics, the spineloid phase will persist metastably beyond the olivine transition equilibrium pressure (Däβler et al., 1996; Tetzlaff and Schmeling, 2009). For example, at a temperature of 1000 °C and assuming the transformation kinetics from Perrillat et al. (2016), the spineloid phase would last over a depths interval of ~ 7 km (**Fig. S5**). Under convective mantle conditions with ~1350 °C adiabatic geotherm this metastability will be reduced and controlled by the interplay between the velocity of the phase transformation and the convective flow (Solomatov and Stevenson, 1994).

Another important issue is the transposition of the present ultrasonic measurements performed at MHz frequencies to the seismological observations in the Hz - mHz range. The shear-wave velocity decrease probed by the ultrasonic waves points to a softening process in the spineloid phase operative at the MHz timescale, coupled to an attenuation of the waveforms. The seismic waves that travel at much lower frequencies will sample these relaxed effective elastic properties, and hence the deceleration of S waves observed in experiments will be also effective at teleseismic periods. In contrast, the attenuation at seismic frequencies cannot be directly inferred from the damping of MHz waveforms since the frequency dependence of the relaxation process is not yet known. However, the contribution of the olivine – wadsleyite transition to the bulk and shear attenuation in the Earth's upper mantle has long been suggested (Jackson, 2007; Li and Weidner, 2008; Ricard et al., 2009) since the phase transformation driven by the propagation of seismic waves in a two-phase loop is a typical source of energy dissipation.

The effect of a transformational softening on the d410 velocity profile, such as the metastable intermediate spineloid phase could create, is qualitatively discussed below and illustrated in **Fig. 5**. The equilibrium elastic profile for an anhydrous pyrolitic mantle composition is the black curve, obtained by Tauzin et al. (2018) through thermodynamical calculations with the Perple_X codes (Connolly, 2005) and the mineral thermoelastic database of Stixrude and Lithgow-Bertelloni (2011). Considering that the fraction of spineloid will be the maximum in the upper part of the loop and will decrease volumetrically with depth as more olivine is transformed into wadsleyite, the occurrence of the spineloid phase will reduce the velocity relative to this equilibrium profile. The amplitude of this velocity drop will

depend on the abundance of the spineloid relative to the olivine and wadsleyite phases, but also on the amount of the non-transforming coexisting minerals, such as pyroxenes and garnet. Hence, the 1.8 – 7.5 % V_s drop observed in the present experiments should be considered as an upper bound. Since the speed of longitudinal waves (V_P) depends partly on the shear modulus we expect that V_p would also decrease to a lesser extent, although it was not possible to measure it in the present experiments. Under geotherm conditions, the impact of this transient softening will be to damp the velocity rise in the uppermost kilometer of the loop red profiles in **Fig. 5**), while in the cold areas of downgoing slabs, where the extent of the spineloid phase will be more pronounced, it could even create a low velocity layer (solid red profile in **Fig.5**). In both settings, the effective thickness of the d410 will be significantly reduced, as detailed hereafter.

Seismic constraints on the d410 structure are mainly from the analysis of secondary reflected or converted seismic waves at the interface (*e.g.* Shearer, 2000). These include P-to-S or S-to-P converted phases from the discontinuity, precursors to PP or SS resulting from underside reflections, as well as P'P' precursors to PKPPKP phases (**Fig. S6**). The reflectivity of these seismic phases, defined as the ratio of amplitude of the reflected or converted wave to the incident wave, depends on the impedance contrast (*i.e.* the product of the velocity and density) across the interface. Hence, the reflectivity of these phases is highly sensitive to the gradients in elastic properties within the loop. The observation of P'$_{410}$P' reflections with ~1 Hz dominant frequency implies that most energy of these waves is reflected from a narrow interface, impossible to reconcile with equilibrium mineralogical models (**Fig. S7**).

The following section is intended to explore the range of amplitude and thickness for the velocity softening that would reproduce the observed seismic reflectivity coefficients and the effective sharpness of the d410. We computed the P'$_{410}$P' reflectivity for various shapes of velocity gradients, and for a range of frequencies between 10^{-2} and 5 Hz. While the Zoeppritz equations are commonly used to compute reflection/conversion coefficients for first-order seismic interfaces, this approach shows some limitations when the discontinuity extends over a significant depth interval as in the case of the olivine high-pressure transformations. When the width of velocity gradients is larger and the shape more complex, the use of reflection/transmission coefficients for first-order interfaces is no longer a good approximation, except at long-periods (Bostock, 1999; Gaherty et al., 1999; Tauzin et al., 2019). We therefore reconstructed the response of velocity profiles by sub-dividing gradients in thin homogeneous layers, and then computing the effective response using a plane-wave matrix algorithm such as designed by Kennett (1983) and Chapman (2003). We modified an

algorithm from Chapman (2003) to calculate the generalized reflection-transmission coefficients from a stack of homogeneous layers (Tauzin et al., 2019). For simplicity, the anelastic attenuation within the layers was not considered here, *i.e.* $Q^{-1} = 0$. We first computed the reflection response of the pyrolite reference equilibrium model along potential temperatures of 600 to 2400 K (**Fig. S7**). The modeled reflection coefficient (RPP) for P'$_{410}$P' phases shows little energy reflection within the 0.6 – 2 s period range. The effect of temperature is to vary the width and velocity contrast across the loop but does not add sharp gradients that may explain the observations of ~1 Hz dominant frequency of P'$_{410}$P' reflected phases. We then constructed models to account for the softening effect that the spineloid phase would produce. We superimposed to the 1600 K pyrolite elastic profile a narrow low-velocity zone of thickness h_1 and perturbations in velocity ΔV_1 and density $\Delta\rho_1$, with an underlying vertical gradient $a_2 = dc/dz$ (where c represents V, and ρ) to connect to the reference elastic structure. **Fig. S8** shows examples of varying ΔV_1, h_1 or a_2 while keeping the other parameters constant. Compared with the simple pyrolitic model, the response is enriched in high frequencies with a peak in the band-pass of analysis of P'$_{410}$P' and P-to-S RF data. The most efficient way to enrich the spectra in high frequencies is to increase the thickness and/or the elastic anomaly within the low-velocity zone. Changing the slope of the underlying gradient has little effect in comparison (**Fig. S8**). Using an appropriate combination of parameters, Δv_1 = -1.5%, h_1 = 2 km and a_2 = 0.2 s^{-1}, we were able to generate a resonance peak close to 1 Hz (**Fig. 6**). Note that given the tradeoffs between the above parameters, this combination is non-unique and a range of models would satisfy the 1 Hz reflectivity (Fig S8). In all these models, the overall effect of the metastable spineloid phase is to broaden the P'$_{410}$P'reflection response toward higher frequencies. This effect could well explain the observation of short-period P'$_{410}$P' phases throughout the globe (**Fig. S6**, Xu *et al.*, 2003).

Finally we explore the detectability of such a narrow (h_1 = 2 km) low-velocity (Δv_1 = -1.5%) layer using receiver functions (RF). We computed P-to-S transmission coefficients (**Fig. 6**) and found a resonance peak in the band pass of RF data at 1.2 Hz. This means that high-frequency RFs could theoretically detect the low velocity layer due to the intrinsic mechanism of the phase transition and investigate its spatial extent. This would nevertheless require to extend the typical period range of RF analysis below 5s periods, and to overcome the current limitations of out-of-phase stacking of the converted arrivals that originate from attenuation, noise and velocity heterogeneities in the upper-mantle.

4. Conclusions

The combination of X-ray diffraction and ultrasonic velocity measurements across the olivine high-pressure transformation evidenced a transient decrease in shear wave velocity which might be related to the spineloid phase reported in previous works. Additional works would be needed to confirm the involvement of this intermediate metastable phase and to measure the evolution of longitudinal wave speeds; which was not possible in this study given the experimental limitations. Such a velocity reduction would affect the seismic signature of the d410, reducing its effective thickness as compared to that predicted by phases equilibrium only. This kinetic effect would be particularly significant in cold mantle environments where transformation kinetics are slow, and would explain the observation of a very sharp discontinuity in cold subduction zones, like Tonga (Yamazaki and Hirahara, 1994; Tibi and Wiens, 2005). The depth of the d410 being also temperature dependent, we hypothesize that the reflectivity of the d410 should be positively correlated with its depth. These results also highlight the importance of investigating dynamics of mantle phase transformations using state-of-the-art *in situ* time resolved probes. It is essential to capture the intermediate metastable phases of the reaction pathway and their bearing on the fine-scale velocity structure of seismic discontinuities.

Acknowledgements

This research was supported by CNRS under INSU-PNP grants to J.P.P. The authors thank Juan Carlos Afonso for providing the elastic profiles associated with mineralogical/seismological models, and Brian L.N. Kennett for insightful advices on the use and development of the plane-wave matrix algorithm. We acknowledge the COMPRES Cell Assembly Development Project supported by COMPRES, the Consortium for Materials Property Research in Earth Sciences under NSF cooperative agreement EAR 01-35554. The Advanced Photon Source – Argonne National Laboratory is acknowledged for the allocation of synchrotron radiation beamtime. GeoSoilEnviroCARS is supported by the National Science Foundation–Earth Sciences (EAR-1128799) and U.S. Department of Energy–Geosciences (DE-FG02-94ER14466). Use of the Advanced Photon Source was supported by the U.S. Department of Energy, Office of Science, Office of Basic Energy Sciences, under contract DE-AC02-06CH11357.

Author contributions

J.P.P. devised the project and performed the synchrotron experiments with J.C., I.D., Z.J. and Y.W. X-ray diffraction and ultrasonic data were analyzed by J.P.P. and J.J. The seismic modeling was conducted by B.T. J.P.P. wrote the paper with the input and discussion from all others co-authors.

FIGURES

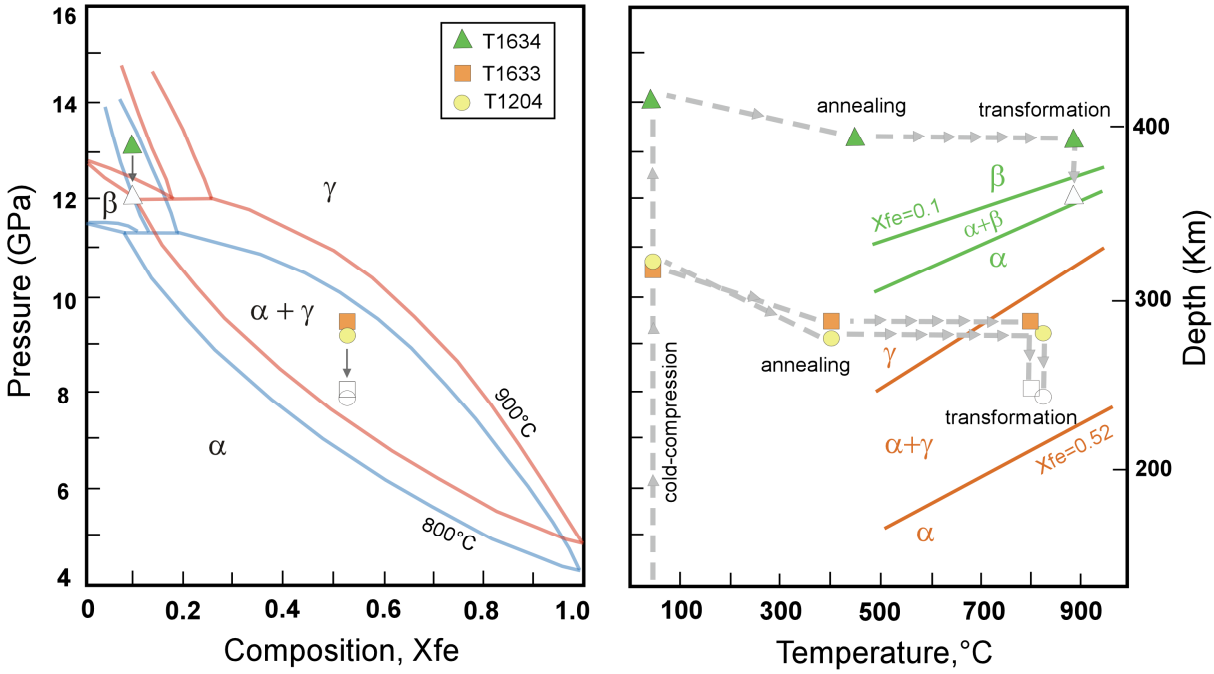

Figure 1 – Phase relations in the $(Mg,Fe)_2SiO_4$ system (left panel, from Akaogi et al., 1989; Katsura and Ito, 1989) and pressure-temperature (P-T) conditions of the present kinetics experiments (right panel). The P-T paths include a cold-compression stage followed by an annealing step at 400 – 500 °C. Temperature is finally jumped to 800 – 890°C for the transformation to occur. In all runs, pressure decreased between the onset of the reaction (filled symbols) and the final measurements (empty symbols), as a result of the negative volume change of the reaction.

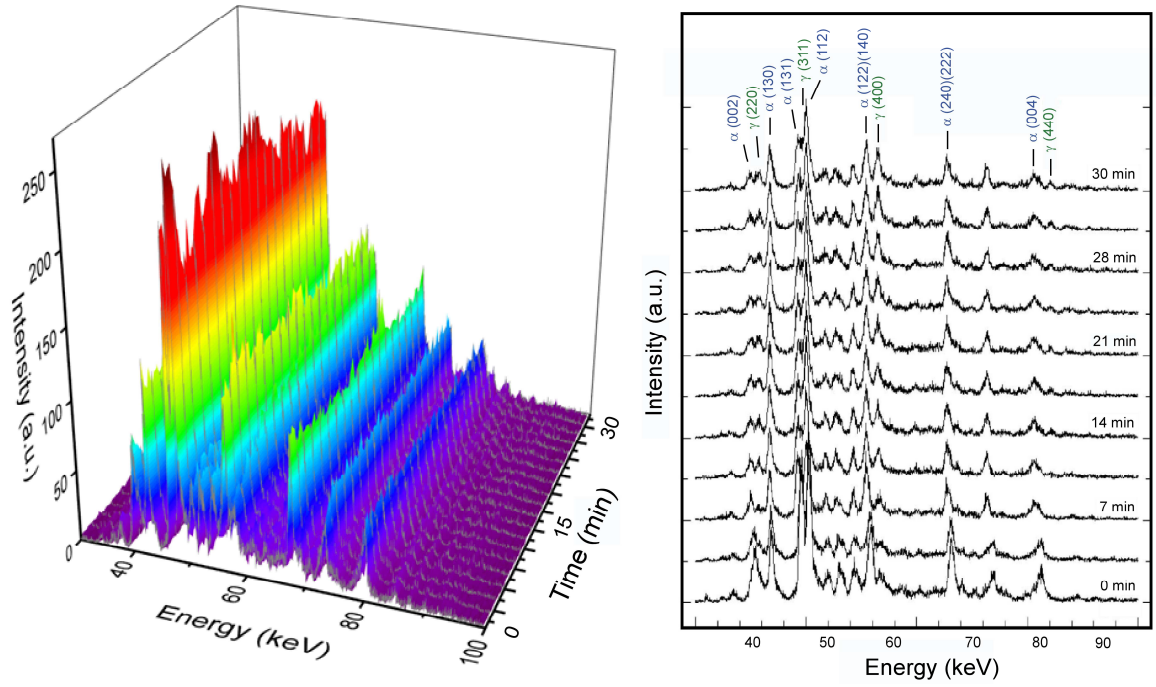

Figure 2 – Time-series of X-ray diffraction patterns for run T1204. Successive spectra show the appearance and growth of ringwoodite (γ) diffraction lines at the expense of olivine (α). (left) whole XRD dataset, and (right) selected patterns.

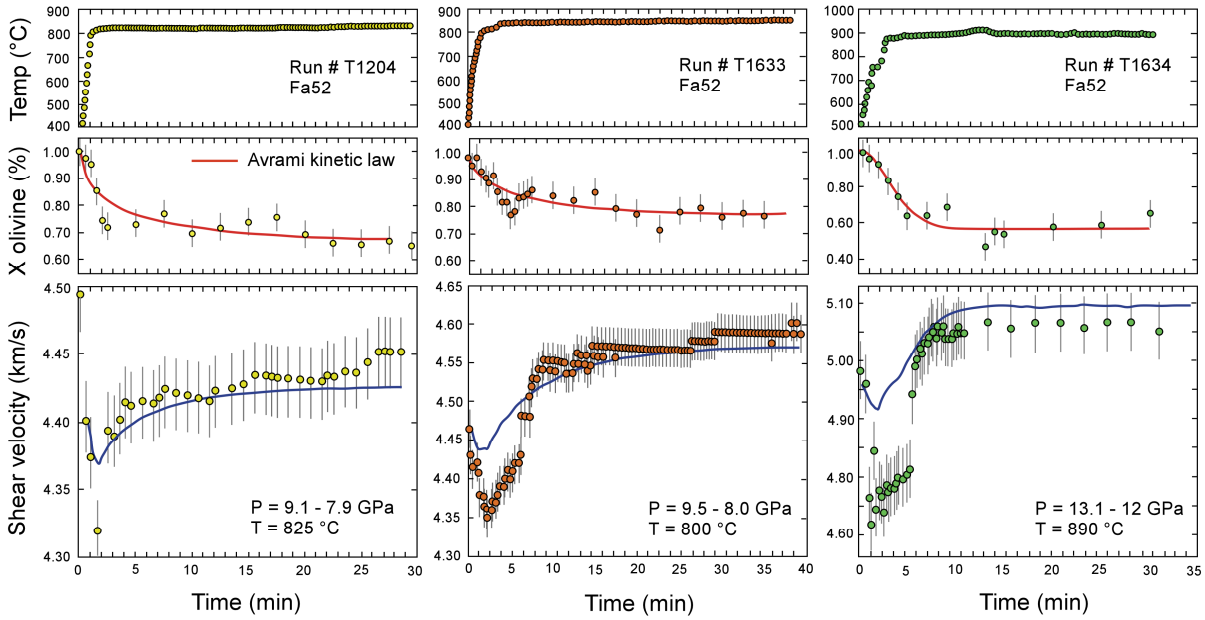

Figure 3 – S-wave velocities as a function of time and reaction progress. (top) Temperature profile as a function of time. (middle) Evolution of olivine fraction estimated from XRD data. The red line is a fit to the Avrami kinetic law $X(t) = 1 - \exp(-kt^n)$, with optimized k and n kinetic parameters. (bottom) Shear velocities along the transformation determined from S-wave travel times and the sample lengths (see Supplementary Table 1 for the raw data). For comparison, velocities were modeled along the same P-T profile using the phase volume fractions determined from XRD and the thermoelastic properties of the individual iron-bearing olivine, wadsleyite and/or ringwoodite phases (see Supplementary Table 2). Modeled velocities (blue curves) exhibit a slight decrease at the onset of reaction due to the temperature rise before stabilization but in all runs the observed shear velocity drops are more pronounced arguing for a reaction-related softening.

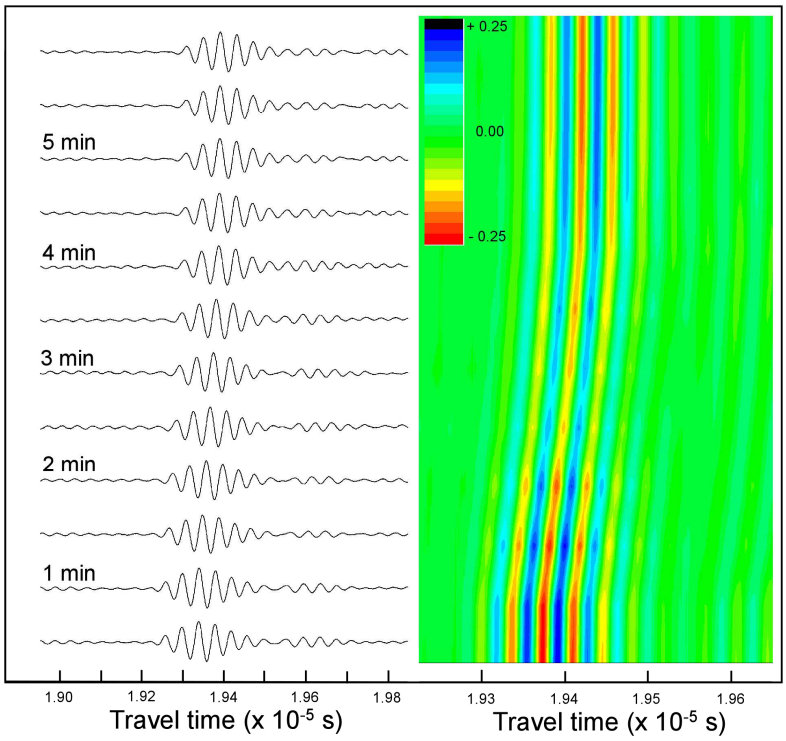

Figure 4 - Successive waveform data of the S-wave echoes as a function of reaction time for sample T1633 (left panel). The lowering of the wave amplitude (colored scale) between 1 and 4 min (right panel) is a possible manifestation of attenuation.

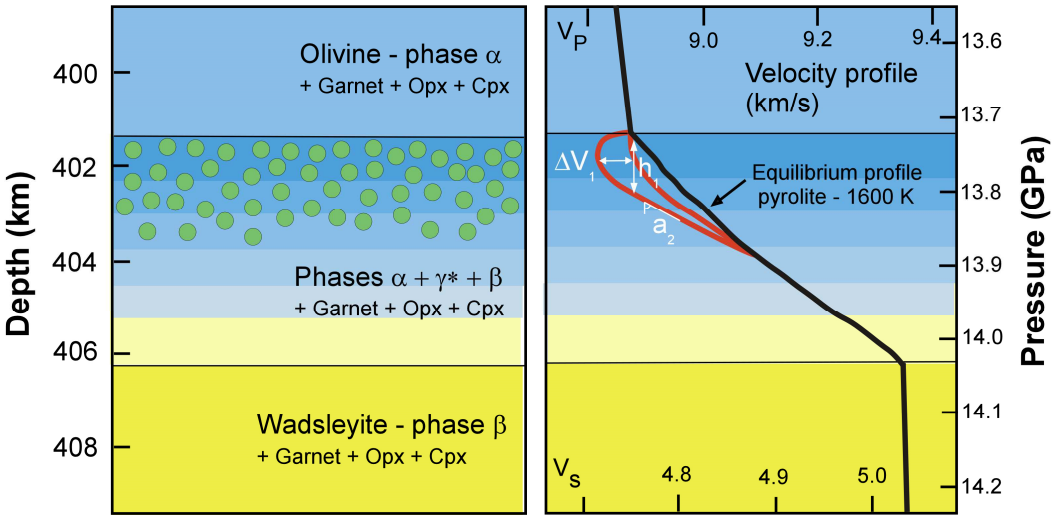

Figure 5 – Schematics of the effect of a transformational softening across the olivine-wadsleyite transformation on the seismic velocity profile

(left panel) Mineral phases as a function of depth for a mantle pyrolitic composition. In the modeling, an intermediate spineloid phase (γ*) coexists with the olivine and wadsleyite phase in the transformation interval. The fraction of this γ* phase (figured as green circles) is maximum in the upper part of the loop and decreases volumetrically with depths as more olivine transformed into wadsleyite. The other non-transforming minerals in equilibrium are garnet, Opx: orthopyroxene and Cpx: clinopyroxene. (right panel) Schematic illustration of the effect of the intermediate γ* phase on the velocity profile. In comparison with the equilibrium profile (black curve), the γ* phase would lead to a softening whose effect would be to lower the velocity rise in the first kilometers of the loop, or even to create a low-velocity layer (red curves).

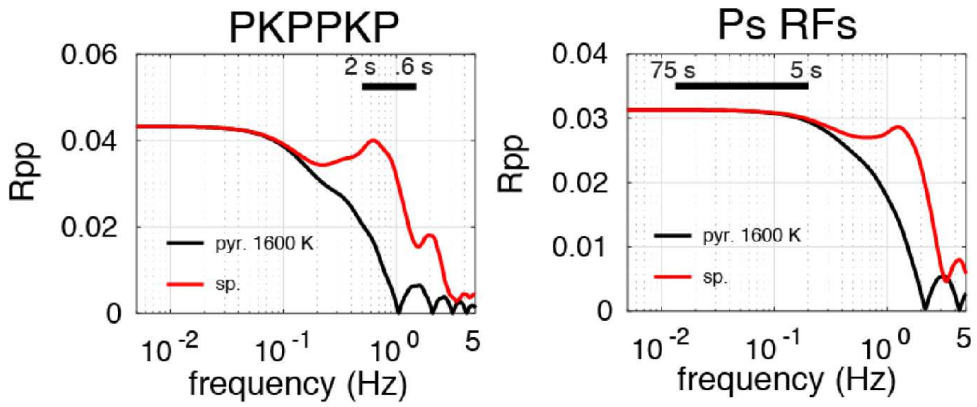

Figure 6 – Effect of a spineloid low-velocity layer on the P'$_{410}$P' (PKPPKP) reflectivity and P-to-S transmission (Ps RFs) coefficients. The reference model in black is obtained from an adiabat with 1600 K potential temperature and a pyrolitic mantle composition (pyr. 1600K). The perturbed model in red corresponding to the presence of the metastable spineloid phase (sp.) is calculated by superimposing a narrow low-velocity zone of thickness h_1 = 2 km, -1.5% perturbations in velocities Δvp_1, Δvs_1 and density $\Delta\rho_1$, and gradient in the underlying velocities a_2 = 0.2 s^{-1}. Compared with the simple pyrolitic model, the spineloid response is expanded toward the high frequencies with a peak in the band-pass of analysis of P'$_{410}$P' and P-to-S RF data (thick black line).

References

Akaogi, M., Ito, E. & Navrotsky, A. 1989. Olivine-modified spinel-spinel transitions in the system Mg_2SiO_4-Fe_2SiO_4: calorimetric measurements, thermochemical calculation, and geophysical application. *J.Geophys.Res*. **94**, 15671-15685.

Bassett,W.A., Skalwold, E.A. 2021. Cation disorder caused by olivine-ringwoodite phase transition mechanism, possible explanation for blue olivine inclusion in a diamond. *Minerals*, 11, 202. https://doi.org/10.3390/min11020202

Benz, H.M., Vidale, J.E. 1993. Sharpness of upper-mantle discontinuities determined from high-frequency reflections. *Nature* **365**, 147-150.

Bostock, M. G. 1999. Seismic waves converted from velocity gradient anomalies in the Earth's upper mantle. *Geophys. J. Int*., **138(3)**, 747-756.

Carpenter, M.A., Salje, E.K.H. 1998. Elastic anomalies in minerals due to structural phase transitions. *European J. Mineral.* **10**, 693-812.

Chandler, B., Devoe, M., Kunz, M., Wenk, H.-R. 2021. Using multigrain crystallography to explore the microstructural evolution of the α-Olivine to γ-ringwoodite transformation and ε-Mg_2SiO_4 at high pressure and temperature. *Minerals*, **11**, 424, doi.org/10.3390/min11040424.

Chapman, C. H. 2003. Yet another elastic plane-wave, layer-matrix algorithm. *Geophys. J. Int.*, **154(1)**, 212-223.

Chen, J., Weidner, D.J., Parise, J.B., Vaughan, M.T., Raterron, P. 2001. Observation of cation reordering during the olivine–spinel transition in fayalite by in situ synchrotron X-ray diffraction at high pressure and temperature. *Phys. Rev. Lett*. **86 (18)**, 4072–4075.

Connolly, J. A. 2005. Computation of phase equilibria by linear programming: a tool for geodynamic modeling and its application to subduction zone decarbonation. *Earth Planet. Sci. Lett.* **236(1-2)**, 524-541.

Däβler, R., Yuen, D.A., Karato, S., Riedel, M.R. 1996. Two-dimensional thermos-kinetic model for the olivine-spinel phase transition in subducting slabs. *Phys. Earth Planet. Int*. **94**, 217-239.

Dziewonski, A.M., Anderson, D.L. 1981. Preliminary reference Earth model. *Phys. Earth Planet. Inter.* **25**, 297–356.

Frost, D.J. 2003. The structure and sharpness of $(Mg,Fe)_2SiO_4$ phase transformations in the transition zone. *Earth Planet. Sci. Lett*. **216**, 313-328.

Furnish, M.D., Bassett, W.A. 1983. Investigation of the mechanism of the olivine–spinel transition in fayalite by synchrotron radiation. *J. Geophys. Res*. **88**, 10333–10341.

Gaherty, J.B., Wang, Y., Jordan, T.H., Weidner, D.J. 1999. Testing plausible upper mantle compositions using fine-scale models of the 410-km discontinuity. *Geophys. Res. Lett*. **26**, 11, 1641-1644.

Guyot, F., Gwanmesia, G.B., Liebermann, R.C. 1991. An olivine to beta phase transformation mechanism in Mg_2SiO_4. *Geophys. Res. Lett*. **18** (**1**), 89–92.

Helffrich, G., Bina, C.R. 1994. Frequency dependence of the visibility and depths of mantle seismic discontinuities. *Geophys. Res. Lett*. **21**, 2613-2626.

Helffrich, G., Wood, B.J. 1996. 410 km discontinuity sharpness and the form of the olivine phase diagram: resolution of apparent seismic contradictions. *Geophys. J. Int*. **126,** 7-12.

Hirth, G., Kohlstedf, D. 2003. Rheology of the upper mantle and the mantle wedge: A view from the experimentalists. in *Inside the Subduction Factory*, *AGU Monograph*, **138**, 83-106.

Hyde B.G., White, T.J. 1982. Structures related to those of spinel and the β-phase, and a possible mechanism for the transformation olivine – spinel, *Zeit. für Kristallo*., **160**, 53-62.

Irifune, T., Isshiki, M. 1998. Iron partitioning in a pyrolite mantle and the nature of the 410-km seismic discontinuity. *Nature* **349**, 409-411.

Jackson, I. 2007. Properties of rocks and minerals – Physical origins of anelasticity and attenuation in rock. in *Treatise in Geophysics*. Eds. G. Schubert Elsevier.

Katsura, T., Ito, E. 1989. Temperature of the transition zone. *Geophys. Res. Lett*. **16**, 425-428.

Katsura, T., Yamada, H., Nishikawa, O., Song, M., Kubo, A., Shinmei, T., Yokoshi, S., Aizawa, Y., Yoshino, T., Walter, M.J., Ito, E. 2004. Olivine-wadsleyite transition in the system $(Mg,Fe)_2SiO_4$. *J. Geophys. Res*.**109**, B02209, doi:10.1029/2003JB002438.

Katsura, T., Yoneda, A., Yamazaki, D., Yoshino, T. Ito, E., 2010. Adiabatic temperature profile in the mantle. *Phys. Earth Planet. Int*., **183** (1-2), 212-218.

Kelbert, A., Schultz, A., Egbert, G., 2009. Global electromagnetic induction constraints on transition-zone water content variations. *Nature*, **460** (7258), 1003-1006.

Kennett, B.N.L. 1983. *Seismic wave propagation in stratified media*. ANU Press, 288pp.

Kennett, B.L.N., Engdahl, E.R., Buland R., 1995. Constraints on seismic velocities in the Earth from travel times. *Geophys. J. Int*., **122**, 108-124.

Kung, J., Li, B., Uchida, T., Wang, Y., Neuville, D., Liebermann, R.C. 2004. In situ measurements of sound velocities and densities accross the orthopyroxene > high-pressure clinopyroxene transition in $MgSiO_3$ at high pressure. *Phys. Earth Planet. Int*. **147**, 27-44.

Lakshtanov, D.L., Sinogeikin, S.V., Litasov, K.D., Prakapenka, V.B., Hellwig, H., Wang, J.W., Sanchez-Valle, C., Perrillat, J.P., Chen, B., Somayazulu, M., Li, J., Ohtani, E., Bass, J.D. 2007. The post-stishovite phase transition in hydrous alumina-bearing SiO_2 in the lower mantle of the earth. *Proc. Nat. Acad. Sci. U.S.A*. **104** (**34**), 13588-13590.

Godec, Y. L., Martinez-Garcia, D., Mezouar, M., Syfosse, G., Itié, J. P., Besson, J. M., 2000. Thermoelastic behaviour of hexagonal graphite-like boron nitride. *High Pres. Res.*, **17**(1), 35-46.

Leinenweber, K.D., Tyburczy, J.A., Sharp, T.G., Soignard, E., Diedrich, T., Petuskey, W.B., Wang, Y., Mosenfelder, J.L. 2012. Cell assemblies for reproducible multi-anvil experiments (the COMPRES assemblies). *Am. Mineral*. **97** (**2-3**), 353–368, doi :10.2138/am.2012.3844

Li, L., Weidner, D.J. 2008. Effect of phase transitions on compressional-wave velocities in the Earth's mantle. *Nature* **454**, 984–986.

Liu, W., Kung, J., Li, B. 2005. Elasticity of San Carlos olivine to 8 GPa and 1073 K. *Geophys. Res. Lett*. **32. L16301**. doi:10.1029/2005GL023453.

Madon, M., Poirier,J.P. 1983. Transmission electron microscope observation of α, β and γ $(Mg,Fe)_2SiO_4$ in shocked meteorites: planar defects and polymorphic transitions, *Phys. Earth Planet. Int*., **33**, 31-44.

Matsui, M., Higo, Y., Okamoto, Y., Irifune, T., Funakoshi, K. I., 2012. Simultaneous sound velocity and density measurements of NaCl at high temperatures and pressures: Application as a primary pressure standard. *Am. Mineral.*, **97**(10), 1670-1675.

Neele, F. 1996. Sharp 400-km discontinuity from short-period P reflections. *Geophys. Res. Lett*. **23**, 419-422.

Pearson, D.G., Brenker, F.E., Nestola, F., McNeill, J., Nasdala, L., Hutchison, M.T., Matveev, S., Mather, K., Silversmit, G., Schmitz, S., Vekeman, B., Vincze, L. 2014. Hydrous mantle transition zone indicated by ringwoodite included within diamond. *Nature* **507**, 221–224.

Perrillat, J.P., Daniel, I., Bolfan-Casanova, N., Chollet, M., Morard, G., Mezouar, M. 2013. Mechanism and kinetics of the α–βtransition in San Carlos olivine $Mg_{1.8}Fe_{0.2}SiO_4$. *J. Geophys. Res.* **118**, 1–10, doi.org/10.1002/jgrb.50061.

Perrillat, J.P., Chollet, M., Durand, S., van de Moortèle, B., Chambat, F., Mezouar, M., Daniel, I. 2016. Kinetics of the olivine–ringwoodite transformation and seismic attenuation in the Earth's mantle transition zone *Earth Planet. Sci. Lett*. **433**, 360-369.

Ricard, Y., Matas, J., Chambat, F. 2009. Seismic attenuation in a phase change coexistence loop. *Phys. Earth Planet. Inter*. **176**, 124–131.

Rosa, A.D., Hilairet, N., Ghosh, S., Perrillat, J.P., Garbarino, G., Merkel, S. 2016. Evolution of grain sizes and orientations during phase transitions in hydrous Mg_2SiO_4. *J. Geophys. Res. Solid Earth* **121** (**10**), 7161-7176.

Shearer, P. M. 2000. Upper mantle seismic discontinuities. in *Earth's Deep Interior: Mineral Physics and Tomography from the Atomic to the Global Scale*. *AGU Monograph* **117**, 115-13.

Sinogeikin, S.V., Bass, J.D., Katsura, T. 2003. Single-crystal elasticity of ringwoodite to high pressures and high temperatures: implications for 520 km seismic discontinuity. *Phys. Earth Planet. Int*. **136**. 41–66.

Solomatov, V.S., Stevenson, D.J. 1994. Can sharp seismic discontinuities be caused by non-equilibrium phase transformations? *Earth Planet. Sci. Lett*. **125**, 269-279.

Stixrude, L. 1997. Structure and sharpness of phase transitions and mantle discontinuities. *J. Geophys. Res.* **102**, 14835-14852.

Stixrude, L., Lithgow-Bertelloni, C. 2011. Thermodynamics of mantle minerals-II. Phase equilibria. *Geophys. J. Int*. **184**(**3**) 1180-1213.

Tauzin, B., Kim, S., Afonso, J. C. 2018. Multiple phase changes in the mantle transition zone beneath northeast Asia: Constraints from teleseismic reflected and converted body waves. *J. Geophys. Res. Solid Earth* **123**(**8**), 6636-6657.

Tauzin, B., Pham, T. S., Tkalčić, H. 2019. Receiver functions from seismic interferometry: A practical guide. *Geophys. J. Int*., **217**, 1-24, doi.org/10.1093/gji/ggz002.

Tetzlaff, M., Schmeling, H. 2009. Time-dependent interaction between subduction dynamics and phase transition kinetics. *Geophys. J. Int.* **178**, 826–844.

Tibi, R., Wiens, D.A. 2005. Detailed structure and sharpness of upper mantle discontinuities in the Tonga subduction zone from regional broadband arrays, *J. Geophys. Res*. **110**, B06313, doi:10.1029/2004JB003433.

Tomioka, N., Okuchi, T. 2017. A new high-pressure form of Mg_2SiO_4 highlighting diffusionless phase transitions of olivine. *Sci. Reports* doi:10.1038/s41598-017-17698-z.

Tomioka, N., Bindi, L., Okuchi, T., Miyahara, M., Iitaka, T., Li, Z., Kawatsu, T., Xie, X., Purevjav, N., Tani, R., Kodama, Y. 2021. Poirierite, a dense metastable polymorph of magnesium iron silicate in shocked meteorites. *Comm. Earth Environment*, *2* (1), 1-8, doi :10.1038/s43247-020-000

Wang, Y., Rivers, M., Sutton, S., Nishiyama, N., Uchida, T., Sanehira, T. 2009. The large-volume high-pressure facility at GSECARS: A « Swiss-army-knife » approach to synchrotron-based experimental studies. *Phys. Earth Planet. Int*. **174**, 270-281.

Wang, W., Walter, M. J., Peng, Y., Redfern, S., Wu, Z., 2019. Constraining olivine abundance and water content of the mantle at the 410-km discontinuity from the elasticity of olivine and wadsleyite. *Earth Planet. Sci. Lett.*, *519*, 1-11.

Wang, S., Chen, T., Cai, N., Qi, X., Fiege, A., Liebermann, R.C., Li, B., 2019. Pressure-induced velocity softening in natural orthopyroxene at mantle temperature. *Am. Mineral*., **104** (8), 1173-1179.

Waszek, L., Tauzin, B., Schmerr, N.C., Ballmer, M.D. and Afonso, J.C., 2021. A poorly mixed mantle transition zone and its thermal state inferred from seismic waves, *Nature Geosci*, **14**, 949–955, doi: 10.1038/s41561-021-00850-w.

Weidner, D.J., Wang, L. 2000. Phase transformations: implications for mantle structure, in *Earth's Deep Interior: Mineral Physics and Tomography From the Atomic to the Global Scale*. *AGU Monograph* **117**, 215-235.

Will, G., Lauterjung, J. 1987. The kinetics of the olivine-spinel transformation in Mg2GeO4 under high pressure and temperature, in *High Pressure Research in Mineral Physics*, Manghnani, M.H. and Syono, Y. (Eds.), Geophysical Monograph, AGU, Washington DC, 177-186.

Wood, B.J. 1995. The effect of H_2O on the 410-kilometer seismic discontinuity. *Science* **268**, 74-76.

Xu, F., Vidale, J. E., Earle, P. S. 2003. Survey of precursors to P′ P′: Fine structure of mantle discontinuities. *J. Geophys. Res.* **108**(B1). doi:10.1029/2001JB000817.

Yamazaki, A., Hirahara, K. 1994. The thickness of upper mantle discontinuities, as inferred from short-period J-array data. *Geophys. Res. Lett*. **21**, 1811– 1814.

Zhang, D., Jackson, J.M., Chen, B., Sturhahn, W., Zhao, J., Yan, J., Caracas, R., 2013. Elasticity and lattice dynamics of enstatite at high pressure. *J. Geophys. Res. Solid Earth*, **118** (8), 4071-4082.

Zhang, J.S., Bass, J.D., 2016. Single-crystal elasticity of natural Fe-bearing orthoenstatite across a high-pressure phase transition. Geophys. Res. Lett., **43** (16), 8473-8481